



Defense Science Quarterly

News about the Science Campaign

Spring 2010

Inside This Issue

- 1 Message from the Director
- 2 The Study of High-Speed Surface Dynamics Using a Pulsed Proton Beam
- 4 Sub-Sonic Thermal Explosions Investigated by Radiography
- 5 Application of a Multiscale Model of Tantalum Deformation at Megabar Pressures
- 7 VarFrame High-Speed Camera System
- 8 Stewardship Science Graduate Fellowship Program
- 9 Publication Highlights
- 10 Highlights and Awards

Message from the Director

Chris Deeney, Defense Science Division

This spring, we have seen a major increase in support for our NNSA programs. The publication of the Nuclear Posture Review and the significant increase in our FY 2011 budget request reinforces our commitment to excellence and motivates us to ensure the Nation's continued confidence in our stewardship program. Our science, technology and engineering programs are at the core of this confidence.

In this issue of the *Defense Science Quarterly*, the continued growth in our scientific knowledge and understanding are discussed in four exciting articles. The first two articles are about using proton radiography as a tool to explore complex hydrodynamics. Just over a decade ago, this technique was in its infancy and now it is a workhorse quantitative measurement tool for the complex, applied to both performance and safety as discussed in the articles. Another technique that has been maturing is the use of laser platforms to infer strength data. The third major article provides a comparison of strength measured on different platforms and compared with multiple models. A new multi-scale model indicates great promise to link different strain-rate regimes. Improved diagnostics remain a major thrust in our program. The new framing camera described in the final article by National Security Technologies, LLC will be a great tool to support a number of our hydrodynamic experiments.

We also feature two graduate fellows: Angelo Signoracci and Luke Roberts. The Stewardship Science Graduate Fellowship Program, as demonstrated by the challenging research being performed by Angelo and Luke, is an inspiration to us all about the future. Never let us forget that as NNSA management and laboratory management, our responsibility is to ensure that we attract a high caliber of early career scientists into our programs. Our national security enterprise wants them to succeed. I had a chance to talk with some of the early career staff and students at Los Alamos National

Laboratory (LANL) when I recently attended their Materials Capability Review. Well done, LANL, for attracting and motivating these impressive individuals. Dr. Allan Hauer and Lois Buitano also recently participated in the Omega Laser Users Group Meeting in Rochester, NY. Yet again, we find a high caliber of early career scientists who enjoy working at an impressive facility. Congratulations to Dr. Robert McCrory and his team for their great work and willingness to gather and research useful feedback.

A number of our scientists have recently been acknowledged by their peers for their achievements. As always, it is a delight when our scientists receive recognition and kudos for their contributions. Congratulations to Dr. Rusty Gray and Professors Henry Kapteyn and Margaret Murnane on their recent awards and professional recognition.

Finally, the Defense Science Division welcomes its newest team member, Dr. Keith LeChien. In his new federal government position, he will apply his excellent technical skills to our program. Dr. LeChien received his Ph.D. in 2006 from the University of Missouri-Columbia in electrical engineering. From 2006 to 2010, he was a member of the technical staff at Sandia National Laboratories, where he was a key contributor in improving laser-triggered gas switch technologies on Z. He will strengthen the capabilities of our team. Welcome, Keith! •



Arthur L. Schawlow & R.W. Wood Prizes

Henry C. Kapteyn and Margaret M. Murnane, JILA, University of Colorado, were the recipients of two prestigious awards this year. They received the American Physical Society's 2010 Arthur L. Schawlow Prize in Laser Science for their pioneering work in the area of ultra-fast laser science. They also received The Optical Society's 2010 R.W. Wood Prize for critical advances in the science and technology of high harmonics generation. Kapteyn and Murnane currently have a grant with NNSA and DOE's Office of Science Joint Program in High Energy Density Laboratory Plasmas program.



Comments

Questions or comments regarding the *Defense Science Quarterly* should be directed to Terri Batuyong, NA-121.1 (Terri.Batuyong@nnsa.doe.gov).

Technical Editor: Christina Coulter

The Study of High-Speed Surface Dynamics Using a Pulsed Proton Beam by W.T. Buttler, D.M. Oro, G. Dimonte, C. Morris, and G. Terrones (Los Alamos National Laboratory)

Los Alamos National Laboratory (LANL) is presently engaged in the development and implementation of ejecta source and transport models for integration into LANL hydrodynamic computer codes. Because the underlying postulate for ejecta formation is that ejecta are produced by a special limiting case of a Richtmyer-Meshkov (RM) instability,^{1,2} where the Atwood number is $A = -1$,³ a key element of the source modeling and transport centers on high-explosive (HE) shocked-Sn validation and verification RM experiments, such as the experimental results presented here.

The FY 2009 experimental package design, seen in Figure 1, incorporated a P025 HE lens and a PBX 9501 booster in contact with a Ti buffer onto which the Sn sample was mounted. The HE was confined within a Delrin cylinder that included a Delrin-capped Lexan tube that permitted inclusion of seven laser Doppler velocimetry probes positioned to monitor the free-surface velocity in four regions and the coincident measurement of the RM bubble and spike velocities.

The Ti buffer had an outer diameter of $d = 76.2$ mm and a thickness of $\tau = 4$ mm, with a 1-mm-deep counter-sunk area on the package center-line that was cut to the Sn target diameter of $d = 42$ mm; the Sn target was epoxied into the counter-sunk region. The average Sn target thickness was $\tau = 2$ mm and had three regions with a sine-wave pattern machined into the surface. The three regions were separated by two flat regions used to determine the shocked surface particle velocity. The three sine-wave areas were defined by three different wavelengths of $\lambda_1 = 0.60$ mm, $\lambda_2 = 2.5$ mm, and $\lambda_3 = 0.60$ mm, with sine-wave amplitudes of $a_1 = 0.025$ mm, $a_2 = 0.10$ mm, and $a_3 = 0.10$ mm. These parameters gave wave-number and amplitude products of $k_1 a_1 = k_2 a_2 = 1/4$, and $k_3 a_3 = 1$.

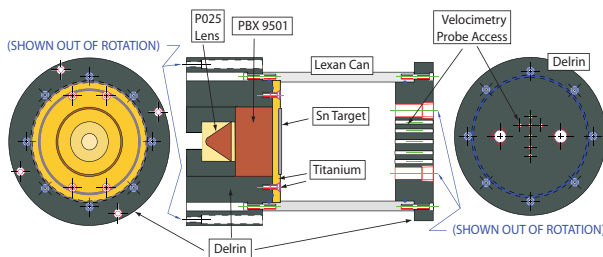


Figure 1: The HE package geometry is shown with the pressure can assembly

Earlier work emphasized the need for the Proton Radiography (pRad) Facility's $\times 3$ magnification capability, which has a resolution of $100 \mu\text{m}$ and a 40 by 40 mm square field of view (FOV), to image ejecta formation. Experimental timing was determined through the use of known HE and detonator function times combined with the expected shockwave pressure P_{SB} and the ejecta

velocity model used to estimate the speeds of the fastest ejecta. The ejecta velocity is based on the Meyer-Blewett model for the RM growth rate,³ namely, the ejecta "spike" velocity is estimated to be

$$u_{spk} = u_{fs} + u_{mb} = u_{fs} + u_{fs} \frac{ka}{2} \left(2 - \frac{u_{fs}}{u_{sh}} \right)$$

where u_{spk} is the fastest spike velocity, u_{mb} is the Meyer-Blewett velocity, u_{fs} is the "free-surface" velocity, ka is the product of the wavenumber and amplitude, and u_{sh} is the velocity of the shockwave within the shocked Sn material. Assuming $P_{SB} \approx 35$ GPa implies $u_{fs} \approx 2.25$ mm/ μs and that $u_{sh} \approx 4.27$ mm/ μs . Using the largest $ka = 1$ for this system gives $u_{spk} \approx 3.9$ mm/ μs . Using the estimated shockwave breakout time together with the FOV and ejecta velocities, 3 image times were grouped early to capture breakout, and the remaining 16 were grouped every 700 ns for the experimental duration.

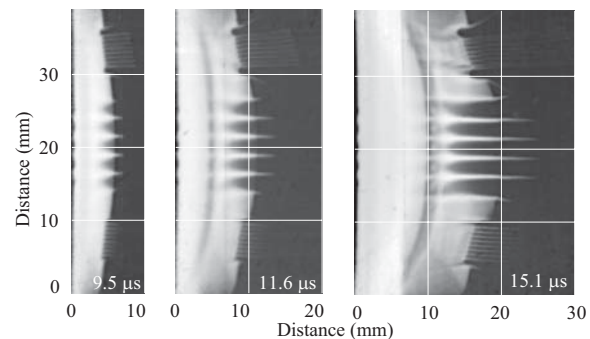


Figure 2: Three of 19 FY 2009 pRad RM images (Shot 371), with image times shown. The instabilities are not fully resolved at this scale and contrast level. However, the salient features that include bubble and spike positions relative to the flat regions are evident.

These preparations led to the vacuum data presented in Figure 2, which shows the short-wavelength, large-amplitude ($ka = 1$) RM spikes travel the fastest, with the short-wavelength and small-amplitude ($ka = 1/4$) traveling at a similar yet lower velocity as the long-wavelength and large amplitude ($ka = 1/4$). The bubbles are also clearly evident and distinguishable from the free-surface velocity that is determined by the flat regions between the sinusoidal perturbations.

Time-series data are presented in Figures 3 and 4. Removed from these data are the long-wavelength regions (these data are not useful because the longer wavelength is on the order of the target thickness τ), and the $\lambda = 600 \mu\text{m}$ regions with $a = 25 \mu\text{m}$ and $a = 100 \mu\text{m}$ are positioned side-by-side. The flat regions that relate u_{fs} were kept, and the time-stamps, which are relative to detonator-breakout, are included in the bottom of each image and are matched as well as possible to the nearest times of other frames. The contrasts in these images are also adjusted to highlight the spike-masses. Because of

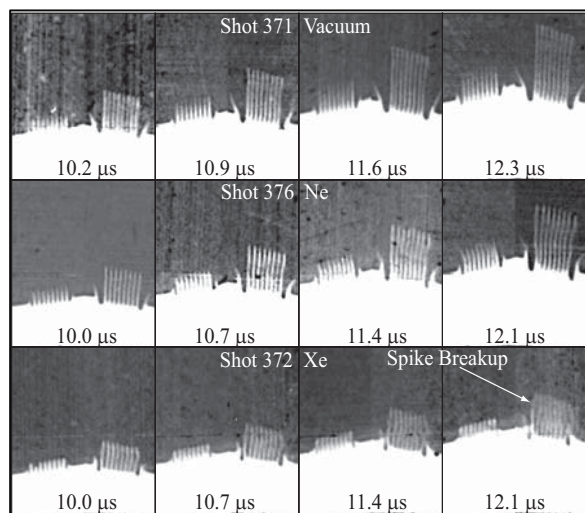


Figure 3: Vacuum, Ne, and Xe pRad RM time-series data, beginning just after shockwave breakout. The Sn is fully liquid on release, and the gas pressure was ~ 4 Atm. for each pressurized experiment. Image times are closely matched.

this, the bubbles are not perfectly resolved, as can be seen in comparisons with Figure 2, whose contrast is nominally set to the proton transmission.

From these data it is seen that the RM spikes in the Ne gas behave much more like the vacuum series than do the spikes in the Xe gas. This is interesting because the viscosity of Ne is about twice the Xe viscosity, i.e., $\eta_{(\text{Ne})} \approx 2\eta_{(\text{Xe})}$. Further, because the density of Xe is about five times the density of Ne, the kinematic viscosity of Ne is about $\times 10$ the kinematic viscosity of Xe: $\eta_{(\text{Ne})}/\rho_{(\text{Ne})} \approx 10 \eta_{(\text{Xe})}/\rho_{(\text{Xe})}$. The implication is that the Weber number $We = \rho_{\text{Sn}} u_{\text{spk}}^2 L / \sigma$ dominates the spike-breakup, where L is the spike tip diameter, and σ the surface tension.

The discussion of particle breakup is important to particle transport in gasses. We have highlighted We , but we also observe that hydro models predict that the RM spike tips will not continue to grow thinner with time, but rather that they will become blunted due to surface tension. This effect is nominally seen at around $11.6 \mu\text{s}$ in the vacuum series, which implies the effect happens in the Ne and Xe series as well, but drag may be stripping liquid Sn off the blunted tips, streaming the material toward adjacent neighbors. This assumption is supported by the fact that the RM spikes appear to breakup in the middle of the spikes in the Ne gas at time $15.1 \mu\text{s}$, and at time $12.1 \mu\text{s}$ in

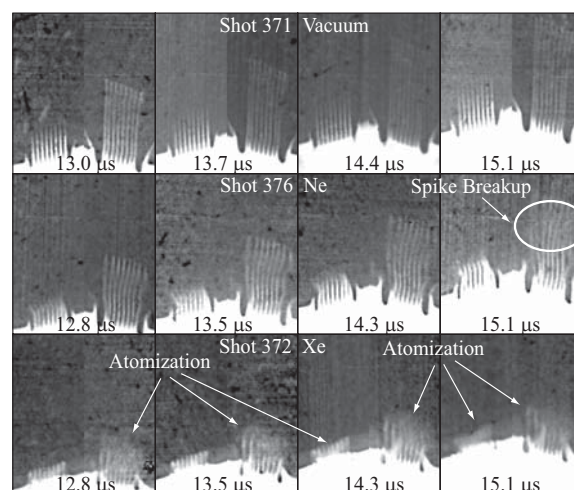


Figure 4: Additional vacuum, Ne, and Xe pRad RM time-series data. Image times are closely matched.

the Xe gas. Close inspection reveals that there may be some evidence of the mass streaming from the fastest Ne spike tips, in the shape of a mach-stem, to their nearby neighbors at time $11.4 \mu\text{s}$.

In conclusion, these observations will be used for code validation and verification studies, and the collection of results to inform FY 2010 experimental packages. For example, it is clear that $\lambda = 2.5 \text{ mm}$ is too long for the $\times 3$ magnifier, and too similar in scale to the coupon thickness, for such data to be of value. The results also show that $\lambda = 600 \mu\text{m}$ is resolvable, and that it is likely that this can be reduced to $\lambda \approx 450 \mu\text{m}$. The amplitudes are relevant and need not be changed, but the coupon thickness can be increased to as much as $\tau = 10 \text{ mm}$. It is also possible to reduce the edge release effects by using a larger diameter booster and lens, especially when combined with momentum trapping concepts that isolate release waves from the central portion of the coupon. Other booster materials, such as PBX 9502 or TNT, can be used to reduce the peak stress, P_{SB} , to levels near 20 GPa, allowing full investigation of other components of our ejecta model development.

¹R.D. Richtmyer, *Commun. Pure Appl. Math* 13, 297 (1960).

²E.E. Meshkov, *Izv. Akad. Nauk SSSR, Mekh. Zhidk. Gaza* 4, 151 (1969) [*Izf. Acad. Sci. USSR Fluid Dynamics* 4, 101 (1969)].

³K.A. Meyer and P. J. Blewett, *Phys. Fluids* 15, 753 (1972).

We acknowledge contributions by Patrick T. Reardon and Machinist Felix P. Garcia of MST-7, and the pRad core team, which are quite extensive. •

NIF Neutron Imaging System Tested with Neutrons at Omega

The lens transfer portion of the National Ignition Facility (NIF) Neutron Imaging System was tested with neutrons for the first time at the Rochester Laboratory for Laser Energetics Omega facility. Ten Omega shots were taken with the new system. Resolution and step wedge measurement were made in three different orientations with respect to the scintillating fiber axis. Camera timing was varied to collect images at initial gamma time (around the 14 MeV peak) and at a down-scatter neutron time. Remaining shots were devoted to flat field measurements. The system will eventually be delivered to NIF.

Sub-Sonic Thermal Explosions Investigated by Radiography by L. Smilowitz, B.F. Henson, B.W. Asay, J.J. Romero, G.P. Grim, A. Saunders, F. Merrill, C. Morris, C. Schwartz, W. McNeil, and pRad Collaboration

Understanding the response of an explosive such as the HMX-based formulation PBX 9501 is critical for being able to predict its behavior in an accident scenario. Despite our detailed knowledge of detonation in this material, we cannot predict the outcome of the same material under conditions of a thermal explosion. The outcome of a particular heating scenario can span the full range of response between a relatively benign pressure burst and a high violence explosion or even steady state detonation. Radiographic imaging of supersonic detonation has been informing that field for over 60 years. However, sub-sonic events present particular challenges that had precluded their observation by radiography. We have developed techniques to overcome those technical difficulties enabling the study of sub-sonic burning in thermal explosions of the PBX 9501 and PBXN-9 using proton radiography.

Radiography provides a measure of the evolution of density caused by material flow and decomposition leading up to ignition and then a measure of the rapid consumption of material during burn propagation subsequent to ignition. The ability to perform these experiments was predicated on several developments: 1) the control of ignition location in a thermal explosion, 2) the prediction of ignition time for a given boundary condition, in some cases the synchronization of the ignition event, and 3) the triggering of external diagnostics synchronous with the breakout of ignition. We have performed a series of thermal explosion experiments at the Proton Radiography (pRad) Facility at Los Alamos National Laboratory exploring two different geometries, two case confinements, and two different HMX-based formulations.

The results of these experiments are sequences of proton transmission images which can be calibrated into material density images and used to study the mechanism by which deflagration occurs. The image below shows one sequence of frames during a thermal explosion in a 1-inch diameter by 1-inch-tall cylinder of PBX 9501 which is encased in 1/8-inch-thick aluminum and heated from heaters wrapped around the aluminum case to a final hold temperature of 205 °C. At this temperature, the time to ignition is approximately 30 minutes. At a time within 1 minute of the ignition time, a laser pulse is applied to within the central ignition volume to synchronize the onset of ignition within a 1-microsecond duration proton pulse window. The onset of ignition is observed by a thermocouple at the center of the explosive and this is used to trigger the acquisition of proton transmission images.

Figure 1 shows proton transmission images taken 20 microseconds apart illustrating the early onset of ignition, the propagation of cracks from the ignition volume outwards to the radial case confinement, and the consumption of the PBX 9501. The grey scale used shows high density (such as the outer aluminum case) in black and lower density in white. The images of density

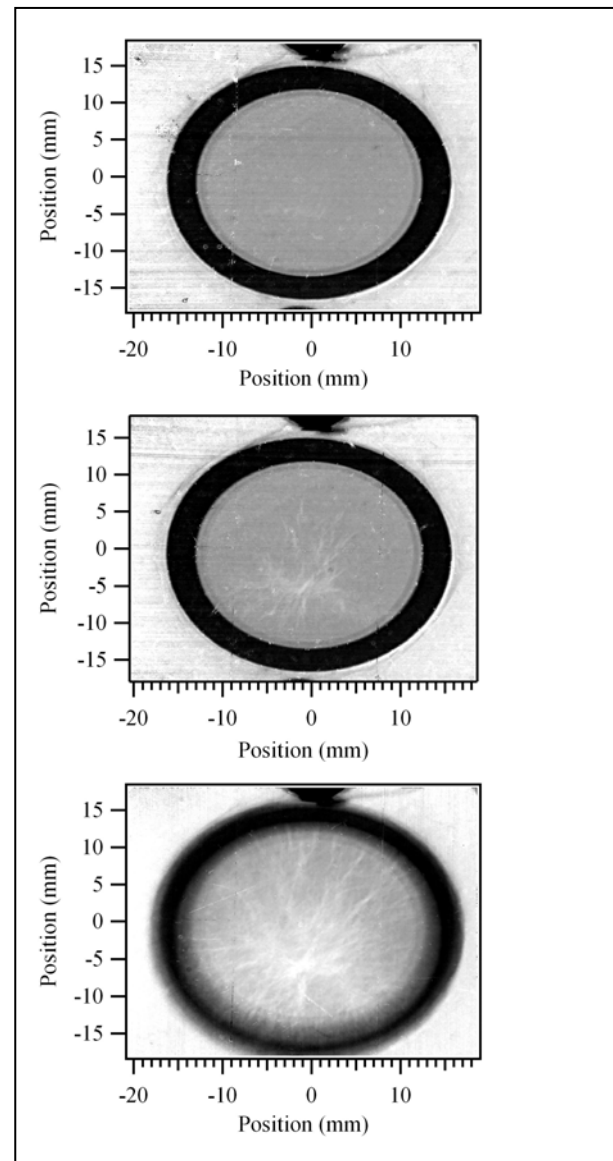


Figure 1: Frame taken just after onset of ignition, followed by ones taken at 20 and 40 microseconds

evolution during thermal explosions in PBX 9501 have been used to develop a model for deflagration. The event observed includes an initial ignition volume of approximately 1-mm radius at the center of the HE. Subsequent to the breakout of ignition, the radial case begins to expand and cracks appear propagating from the central ignition volume out to the case walls. These cracks propagate to the walls 1/2 inch away within approximately 10 microseconds. A convective burn propagates outward from the central ignition volume at approximately 200 m/s lighting the material and consuming 10-15% of the explosive. Following the convective lighting, the material is consumed over the following tens of microseconds by a slower conductive

consumption. These observations and measured velocities are captured in a model used to simulate the radiographic data.

Proton radiography of thermal explosions has yielded a mechanism for deflagration propagation which consists of both convective and conductive processes. Further work is underway to image the phenomena involved in the deflagration to detonation transition.

References

- 1) L. Smilowitz, B.F. Henson, M.M. Sandstrom, J.J. Romero, B.W. Asay, Applied Physics Letters 90 (2007).
- 2) L. Smilowitz et al., Direct Observation of the Phenomenology of a Solid Thermal Explosion Using Time-Resolved Proton Radiography, Physical Review Letters 100 (2008).
- 3) J.W. Tringe, J.D. Molitoris et al., Time-sequenced X-ray Observation of a Thermal Explosion. In AP5 Shock Compression of Condensed Matter, AIP: Nashville, TN, 2009. •

Application of a Multiscale Model of Tantalum Deformation at Megabar Pressures by R. Cavallo, H. Park, N. Barton, B. Remington, S. Pollaine, S. Prsbrey, J. Bernier, M. May, B. Maddox, D. Swift and the Materials Integrated Experimental Team (Lawrence Livermore National Laboratory), R. Becker (Army Research Laboratory) and R. Olson (Los Alamos National Laboratory)

A new multiscale simulation tool has been developed to model the strength of tantalum under high-pressure dynamic compression. This new model combines simulations at multiple length scales to explain macroscopic properties of materials. Previously known continuum models of material response under load have built upon a mixture of theoretical physics and experimental phenomenology. Experimental data, typically measured at static pressures, are used as a means of calibration to construct models that parameterize the material properties, e.g., yield stress, work hardening, strain-rate dependence, etc. The pressure dependence for most models enters through the shear modulus, which is used to scale the flow stress. When these models are applied to data taken far outside the calibrated regions of phase space (e.g., strain rate or pressure), they often diverge in their predicted behavior of material deformation.

The new multiscale model, developed at Lawrence Livermore National Laboratory (LLNL), starts with interatomic quantum mechanical potential and is based on the motion and multiplication of dislocations¹. The basis for the macroscale model is plastic deformation by phonon drag and thermally activated dislocation motion and strain hardening resulting from elastic interactions among dislocations. The dislocation density, ρ , and dislocation velocity, v , are connected to the plastic strain rate, $\dot{\epsilon}^p$, via Orowan's equation: $\dot{\epsilon}^p = \frac{\rho b v}{M}$, where b is the Burger's vector, the shear magnitude associated with a dislocation, and M is the Taylor factor, which accounts for geometric effects in how slip systems accommodate the deformation. The evolution of the dislocation density and velocity is carried out in the continuum model by parameterized fits to smaller scale simulations, each informed by calculations on smaller length scales down to atomistic dimensions.

We apply this new model for tantalum to two sets of experiments and compare the results with more traditional models. The experiments are based on the Barnes² technique in which a low density material loads against a metal surface containing a pre-imposed rippled pattern. The loaded sample is Rayleigh-Taylor unstable and the rippled amplitudes grow with time. The rate of

growth differs depending on the material strength, with stronger materials growing less, even to the point of saturation. One set of experiments was conducted at the pRad facility at LANSCE at Los Alamos National Laboratory in 2007 using high-explosive (HE)-driven tantalum samples. The other set of experiments was done at the Omega laser at the Laboratory for Laser Energetics at the University of Rochester, which used high-powered lasers to create plasmas to dynamically compress a rippled tantalum sample (see e.g., Park et al.^{3,4}). The two techniques provide data at different pressures and strain rates: the HE technique drives the samples at around $2 \times 10^5 \text{ s}^{-1}$ strain rate and pressures near 500 kbar, while the laser technique hits strain rates around $2 \times 10^7 \text{ s}^{-1}$ and pressures close to 1.4 Mbar.

The most recent laser experiments were conducted in February 2010 and we present a sample of the data in Figure 1, which shows a face-on radiograph at a time of 65 ns after the laser was turned on. From this radiograph, we measure the growth factor which is defined to be the change in amplitude of the ripples relative to their initial amplitude. Figure 2 shows the resulting growth factors along with various model fits. The error bars are typically

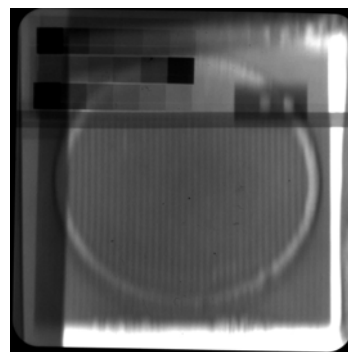


Figure 1: Face-on 22 keV x-ray radiograph of a rippled sample target of tantalum at 65 ns after initial laser pulse. The driven ripples constitute the center of the image, while the upper portion of the image contains added features (stepped filters and knife-edge resolution block) to aid in the extraction of the growth factor. The ripple amplitudes are derived from transmission contrast between peak and valley of the ripple regions.

20-25%. Only the multiscale model predictions match the experimental measurements. The growth factors via the HE technique are determined from multiple side-on proton radiography images and, thus, provide a full growth curve per single experiment. A sample growth curve is shown in Figure 3, also with various model fits and error bars estimated at 25%. It should be noted that by 7.5 μs the growth in this sample has exceeded the initial target thickness indicating that localizations not captured in the overall simulation have probably become dominant, i.e., the target is likely breaking up.

Application of the multiscale dislocation dynamics model as implemented in the Ares⁵ hydrodynamics code shows excellent agreement with both the pRad and Omega data. We also compare the Steinberg-Lund⁶ (SL), Preston-Tonks-Wallace⁷ (PTW), and Steinberg-Guinan⁸ (SG) models with the data. The PTW and SG models provide good fits to the pRad data but overpredict the growth (underestimate the strength) on the laser platform. The SL model underpredicts the pRad data and overpredicts the Omega data. The excellent agreement of the multiscale model with the data over two orders of magnitude in strain rate and more than a factor of two in pressure lends credibility to the model. We will continue to stress the model by conducting experiments at 5 Mbars and beyond at the National Ignition Facility at LLNL in the near future.

¹ R. Becker et al., A Tantalum Strength Model using Multiscale Approach: Version 2, September 2009, LLNL-TR-417075.
² J.F. Barnes, P.J. Blewett, R.G. McQueen, K.A. Myer, and D. Vernable, Taylor Instab. in Solids, J. Appl. Phys. 45, 727 (1974).
³ H.-S. Park et al., Viscous Rayleigh-Taylor Instability Experiments at High Pressure and Strain Rate, Phys. Rev. Lett. 104, 135504 (2010).
⁴ H.-S. Park et al., Strong Stabilization of the Rayleigh-Taylor Instability by Material Strength at Megabar Pressures, Phys. Plasmas 17, 056314 (2010).
⁵ G. Bazan, in Proceedings from the 2nd International Workshop on Laboratory Astrophysics with Intense Lasers, UCRL-ID-131978, (Lawrence Livermore National Laboratory, CA), 42 (1998).
⁶ D.J. Steinberg and C.M. Lund, A Constitutive Model for Strain Rates from 10^{-4} to 10^6 s^{-1} , J. Appl. Phys. 65, 1528 (1989).
⁷ D.L. Preston, D.L. Tonks, and D.C. Wallace, Model of Plastic Deformation for Extreme Loading Conditions, J. Appl. Phys. 93, 211 (2003).
⁸ D.J. Steinberg, S.G. Cochran, and M.W. Guinan, A Constitutive Model for Metals Applicable at High-Strain Rate, J. Appl. Phys. 51, 1498. ●

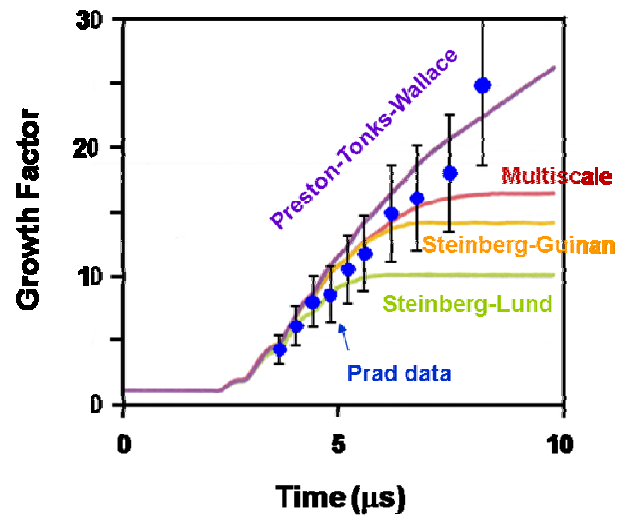


Figure 2: Comparison of various model predictions with growth factor data obtained at the Omega laser facility, Rochester, NY, in 2009 and 2010. The data reach peak pressures between 1.2 and 1.4 Mbar and average strain rates around $2 \times 10^7 \text{ s}^{-1}$.

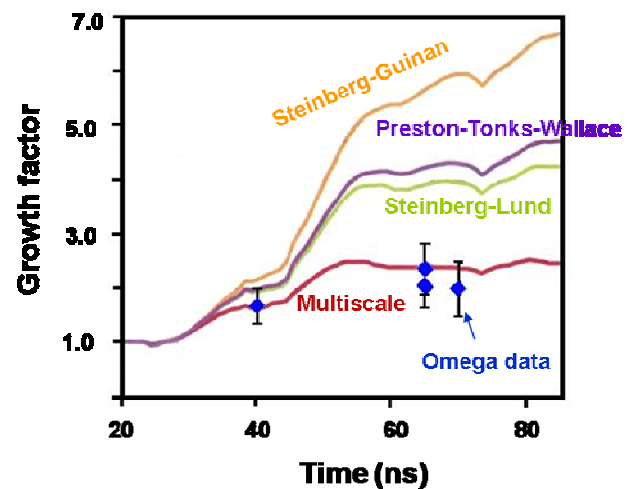


Figure 3: Comparison of various model predictions with growth factor data obtained at the pRad facility, Los Alamos, NM, in 2007. The data reach a peak pressure of 500 kbar and an average strain rate of $2 \times 10^5 \text{ s}^{-1}$.

Forty-nine Consecutive Z Shots Without a Gas-switch Prefire

As of mid April, the newly upgraded laser-triggered gas switch delivered 49 consecutive Z shots without a single gas-switch prefire (shots 2013 to 2061). This is equivalent to 1764 switch-shots (the number of switches multiplied by the number of shots), which suggests the prefire rate is ~0.06%. This advance has enabled four Z shots per week, since it has eliminated 7 man-hours per week of maintenance. We are developing critical refurbishment techniques to ensure sustained performance at this level. In the coming months, we will test two next-generation switch designs that have been structurally qualified through a series of offline tests that simulate the approximately 200-m/s² acceleration experienced by a switch during a typical Z shot. Both of the new designs are expected to reduce the prefire rate by an additional factor of 2 and the machine timing spread by a factor of 1.5, while increasing gas-switch lifetime. — K.R. LeChien, W.A. Stygar, M.E. Savage, G.R. McKee, M.R. Lopez, J.L. Porter, and M.A. Sweeney (Sandia National Laboratories) and D.S. Artery, M.J. Baremore, P.A. Jones S.A. Roznowski, P.E. Wakeland, and S.D. White (Ktech Corporation).

VarFrame High-Speed Camera System by Matthew Martin and David Glass, National Security Technologies, LLC (NSTec)

NSTec completed a VarFrame camera design and deployed it at the Nevada Test Site (Figure 1). The camera design achieves several technologically competitive goals, having a maximum frame rate of 6.6 million frames per second, a low inter-frame time of 100 nsec, and a variable frame count of 1 to 25 frames.



Figure 1: NSTec's VarFrame camera has a variable frame count of 1 to 25 frames at 6.6 million frames per second

Tube-based imaging cameras have long been a staple of weapons diagnostics. Designed around an electrostatic image tube, a framing camera images the light present during each frame at the photocathode onto the tube's phosphor. The phosphor persistence allows the camera to display multiple frames on the phosphor at one time. During this persistence, a Charge-Coupled Device (CCD) camera is triggered and the analog image is collected digitally. The tube functions by converting photons to electrons at the negatively charged photocathode. The electrons move quickly toward the more positive charge of the phosphor. Two sets of deflection plates skew the electron's path in horizontal and vertical (x axis and y axis, respectively) directions. Hence, each frame's electrons bombard the phosphor surface at a controlled location defined by the voltages on the deflection plates. To prevent the phosphor from being exposed between frames, the image tube is gated off between exposures.

The VarFrame camera's easily configurable frame timing and number, high frame rate, and ease of use for remote applications are features that are well-suited to high-speed imaging applications, including subcritical high-explosive experiments, Powder Gun experiments, and proton radiography beam diagnostics.

The VarFrame camera allows a user on-the-fly selection of 1 to 25 frames (Figures 2 and 3) in any configuration up to five columns and five rows. The timing systems are completely integrated into the camera, minimizing the need for supporting hardware.

The Linux-based control software runs on an embedded computer board, allowing a control computer with Ethernet access and a Web browser to remotely monitor and manipulate the camera's functions. The embedded

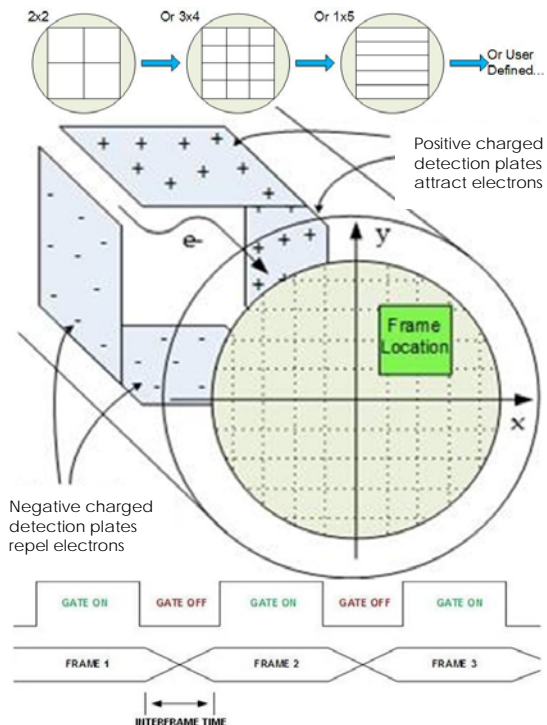


Figure 2: The framing control allows Graphical User Interface (GUI) manipulation of interframe time, frame count, and exposure

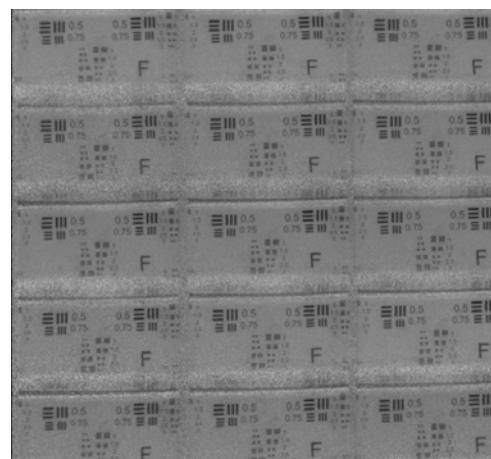


Figure 3: Sample 15-frame image of a resolution test pattern

microprocessor design allows the remote device to maintain settings without remote communication with the host. All settings on the camera are controlled and updated in a real-time browser-based user interface, providing a seamless control experience for the user. The rich client operator control runs in Adobe Flash Player, commonly embedded in most Windows, Macintosh, and Linux browsers. Most desktops are capable of camera control with no software installation. •

Stewardship Science Graduate Fellowship (SSGF) Program



Luke Roberts, a doctoral student in high-energy astrophysics at the University of California-Santa Cruz, is studying how the neutrino-driven wind (NDW) that follows a core-collapse supernova may contribute to the formation of elements heavier than iron. Such winds, arising from the

surface of newborn neutron stars, could contribute significantly to the integrated nucleosynthesis of supernovae.

In a paper recently submitted to *The Astrophysical Journal* (<http://arxiv.org/abs/1004.4916>), the third-year NNSA Stewardship Science Graduate Fellow Roberts describes time-dependent hydrodynamic numerical calculations of nucleosynthesis in the NDW. The calculations coupled accurate weak-interaction physics to a full nuclear-reaction network. Previous NDW studies have used simplified dynamics or nuclear physics, say Roberts, Stan Woosley (his doctoral adviser), and Robert Hoffman, Lawrence Livermore National Laboratory.

The researchers drew on neutrino luminosity histories from two previous supernova models to calculate the dynamics and nucleosynthesis of the entire NDW for the first time. The yields of the wind were then combined with the results of a calculation of the nuclear yields from the rest of the supernova. They find that, when the Milky Way was young, NDW may have contributed significantly to the abundances of strontium, yttrium and zirconium. This could have observable consequences in low-metallicity halo stars. They also developed analytic models of the wind dynamics and nucleosynthesis and found agreement with their numerical models.

The calculations found it unlikely that the r-process occurs in a NDW unless something causes significant deviation from a purely neutrino-driven wind. The r-process involves neutron capture on heavy seed nuclei followed by beta decays. This process can produce nuclei as heavy as uranium and where it occurs is one of the major unsolved problems in nuclear astrophysics. The results of the wind calculations are sensitive to small changes in neutrino temperatures and interaction rates, and to the mass of the progenitor star; however, the researchers note that it's likely that nucleosynthesis in the NDW will vary significantly from event to event.

Roberts' practicum research at Los Alamos National Laboratory in 2009 contributes to his NDW research. Under Sanjay Reddy, he developed a computer code to simulate the early evolution of neutron stars. The general relativistic neutrino transport/stellar structure code uses advanced microphysics for the nuclear equation of state (EOS) and neutrino opacities. The code also implemented a one-dimensional prescription for energy transport by convection to characterize the effects of hydrodynamic instabilities in the young neutron star's interior. The results could help elucidate how hydrodynamic instabilities and the nuclear EOS affect the spectra and luminosities of emitted neutrinos. This will provide more accurate input to the NDW nucleosynthesis calculations Roberts and collaborators performed.



Angelo Signoracci, also a third-year fellow, is working with Alex Brown of Michigan State University (MSU) on mathematical "horticulture" that could provide a better understanding of the low-energy properties of nuclei. He is exploring a novel approach to create a successful hybrid of the shell

model or configuration interaction (CI) and energy density functional (EDF) methods to perform the calculations.

CI is more accurate and includes all correlations in a model space, but it becomes numerically expensive as nuclear mass increases and is limited to specific regions of the nuclear chart. EDF calculates the entire nuclear chart with one parameterization at low numerical cost. However, it has limited accuracy, a lack of universal parameterization, and can calculate only certain states. This combination could deliver the first accurate calculations of the properties of many nuclei for comparison with experiments and predictions to unknown nuclei.

CI and EDF both came into play during Signoracci's practicum at Lawrence Livermore National Laboratory in 2008. Working under W. Erich Ormand, Signoracci parallelized the shell-model code NuShellX to run more efficiently, improving calculation times by an order of magnitude. Using EDF, he renormalized a realistic nucleon-nucleon potential to the specific case of ^{68}Ni , then calculated the isotope's binding energy and single particle energies. He used the renormalized interaction as an input to a CI calculation to produce level schemes of $^{67, 68, 69}\text{Ni}$, ^{67}Co , and ^{69}Cu for comparison with experiment and binding energy calculations. His preliminary calculations disagreed with existing data, requiring improvements in his ongoing work. In later research¹ using CI calculations, Signoracci and his colleagues probed the spectroscopic properties of argon isotopes.

In previous results, measured spectroscopic factors (SF) fell by up to 75% relative to shell model predictions in one-nucleon knockout reactions for strongly bound valence nucleons, the paper says. But some studies predict smaller effects.

Signoracci and his colleagues used (p,d) single-nucleon transfer reactions as an alternative spectroscopic probe to extract SF for proton-rich ^{34}Ar and neutron-rich ^{46}Ar . They analyzed the experimental results with two approaches and found them consistent with systems of SF obtained from transfer reactions on stable nuclei, but inconsistent with trends found in knockout reactions. Their comparison of SF for ^{34}Ar and ^{46}Ar suggest that correlations, which usually reduce SF, don't depend strongly on neutron-proton nuclear asymmetry in this isotope region, as knockout reactions suggest. Their results also pose questions about the mechanisms of transfer and knockout reactions used to probe nucleon correlations in nuclei with unusual isospin asymmetries.

¹ Phys. Rev. Lett. 104, 112701 (2010)

Publication Highlights by Douglas Drake

This section highlights recent publications in high-impact scientific journals of research supported by the NNSA Science Campaigns.

National Ignition Campaign Hohlräum Energetics, N.B. Meezan et al., Lawrence Livermore National Laboratory and Los Alamos National Laboratory, *Physics of Plasmas* 17, March 17, 2010

This paper reports on the results of the first critical series of experiments on the newly operational National Ignition Facility (NIF). As noted in the paper, successful indirect drive ignition on the NIF will require driving the implosion capsule to high velocity without heating the fuel material excessively. In addition, the target must be driven symmetrically to achieve a round imploded core, avoiding quenching of the central hot spot by mixing with the surrounding cold, dense fuel. The goals of this first series of experiments on the NIF were intended to demonstrate that these essential conditions for ignition can be achieved by 1) measuring laser absorption in the hohlraum, 2) measuring the x-ray radiation flux on the surrogate capsule, 3) acquiring quantitative measures of laser absorption and resulting x-ray flux, and 4) determining whether the hohlraum performance is consistent with ignition requirements. To achieve these goals, it was essential to show that the required drive and symmetry could be delivered without excessive backscatter of the laser light due to laser-plasma interactions (LPI) such as stimulated Raman backscatter (SRS) and stimulated Brillouin backscatter (SBS). Levels of backscatter above 10% are considered too high to achieve ignition.

The target used in the experiments was designed so that the performance and plasma conditions were similar to those of a 1.2 MJ ignition hohlraum while operating at a lower laser energy of 500 to 750 kJ. This was achieved by scaling down the size of the target by a factor of 0.78. The initial subcampaigns in the series were designed to demonstrate that the entire suite of diagnostics could be operated simultaneously on one shot. These experiments were carried out at room temperature to avoid the additional complications of cryogenic operations. It was possible to use a neopentane (C₅H₁₂) gas fill in these "warm" experiments. The initial results were encouraging; highly symmetric implosions were achieved with backscatter well below the critical limits.

Following the success of these shots with warm gas fill, a series of shots were fielded using cryogenic hohlraums filled with an 80%/20% hydrogen helium mixture. These were apparently the first successful experiments with laser-driven gas-filled hohlraums, as previous attempts to shoot such targets on NOVA and OMEGA suffered from condensation. However, on the first shot, the level of SRS increased from the 6% recorded in the warm experiments to 19%, demonstrating that plasma composition strongly affects SRS. The experimenters reasoned that a higher Z gas fill, resulting in a higher plasma electron temperature, might decrease SRS. The highest Z gas that could be used at the extremely low temperatures

required in the cryogenic experiments without condensation is helium. When a 100% helium fill was tried, the SRS in the critical inner cone of laser beams was found to drop by half from 18% backscatter to about 9%, within the limits required for ignition.

Based on the results of this first round of energetics experiments on the NIF, it was concluded that we are on the path to a hohlraum design that will successfully ignite using 1.2 to 1.5 MJ of laser energy.

Viscous Rayleigh-Taylor Instability Experiments at High Pressure and Strain Rate, H. Park et al., Lawrence Livermore National Laboratory, *Physical Review Letters* 104, April 2, 2010

In the first numerical studies of inertial confinement fusion, models were typically limited to one dimension because of limitations in computer power. These early models predicted ignition at much lower driver energies than are actually required because they were blind to 2-D and 3-D effects which can result in asymmetric target implosions, quenching the fusion burn process. The Rayleigh-Taylor (RT) instability is a major factor in driving these asymmetries. It is always present when a light fluid accelerates a heavier one, or, equivalently, when the density gradient and acceleration are in opposite directions. When this happens, small surface perturbations on the surface between the two fluids will tend to grow, causing the formation of "bubbles" of low density fluid rising into the higher density regions, and "spikes" of high density material moving in the opposite direction. Since the significance of the phenomenon was realized, there have been constant efforts to find ways to control it. These have included fabrication of ultra-smooth target surfaces, the development of various techniques for achieving highly uniform laser beams, and attempts to carefully control material temperatures and pressures during the implosion process. There is always room for more improvement, and recent experiments and numerical simulations carried out by a team from Lawrence Livermore National Laboratory (LLNL) at the University of Rochester's OMEGA laser facility have demonstrated a promising new approach. High fluid viscosities slow the rate of growth of the RT instability. They seek to take advantage of this by introducing what they call "effective lattice viscosity by phonon drag." This phonon drag effect is predicted to occur at high pressure and strain rates when the dense material is kept below melt temperatures. Using vanadium samples with artificially rippled surfaces, the LLNL team successfully demonstrated that significant reductions from "classical" growth rates in the RT instability can be achieved using the phonon drag mechanism.

Applied Spectroscopy in Pulsed Power Plasmas, G.A. Rochau and J.E. Bailey, *Sandia National Laboratories*, Y. Maron, *Weizmann Institute of Science, Israel*, *Physics of Plasmas* Vol. 17, No. 5, March 11, 2010

In this review paper, the authors discuss the applications of applied spectroscopy, a diagnostic tool that has been used to address a variety of challenging pulsed power

science problems in Z experiments. Applied spectroscopy is based on the fact that the conditions and environment of a plasma affect the ionization state of the constituent elements, the bound atomic energy states, and the distribution of electrons among the bound states. This makes it possible to infer a broad range of plasma conditions by observing the emission or absorption spectra, including the materials present, electron temperature, ion temperature, electron density, ion velocity, and electric and magnetic field strengths. The authors discuss examples of these fundamental measurements across three main categories: the determination of magnetic field penetration in plasma, the determination of electric fields in non-neutral plasma, and the determination of plasma conditions in HED plasmas.

The discussion relating to HED plasmas focuses on recent experiments at Sandia's Z pulsed power facility, in which spectroscopic data has proved invaluable in a host of recent ground breaking experiments. The authors describe in detail the application of spectroscopic diagnostics to radiating shock experiments with dynamic hohlraums. These targets can deliver high power x-ray pulses for a variety of HED physics applications, including radiative transfer, opacity measurements, and ICF. In future work on Z, experimenters will seek to develop challenging new applications of spectroscopy to HED plasmas, including the extension of magnetic field measurements to high density, nonuniform, and turbulent plasmas and techniques to determine the time-dependent spatial distribution of conditions in complex plasmas. •

Highlights and Awards

¹³²Sn Verified as Doubly-Magic Number Nucleus by Team from SSAA Center by Mike Kreisler

The nuclear shell model (Nobel Prize 1963) explains why particular ("magic") numbers of protons and/or neutrons in a nucleus have large binding energies compared to their neighboring isotopes in a manner analogous to the shell structure of electrons in an atom. This elegant model is fundamental to our understanding of the abundances of elements in the galaxy. As the model is tested against experimental observations, it can be used to extrapolate theoretical models beyond the reach of current experimental facilities, helping to address how elements heavier than iron were created in the explosion of stars.

The isotope of tin, ¹³²Sn, with 50 protons and 82 neutrons, is an example of a doubly-magic nucleus as both the proton and neutron numbers are "magic". However, it has proved almost impossible to verify that it is such a state or to study the characteristics of the nuclear states formed when an additional neutron is added because ¹³²Sn lives for only 40 seconds once it is created in the fission of a uranium atom.

A team of scientists, supported in part through the SSAA Center for Excellence for Radioactive Ion Beam Studies for Stewardship Science, has made the critical measurements both establishing ¹³²Sn as a doubly-magic nucleus and determining the characteristics of the single-particle states in ¹³³Sn that lie just above the shell closures (*Nature* Vol. 465, No. 7297, May 27, 2010). They were able to show that the properties of these single particle states are largely determined by the last unpaired neutron.

This important work was achieved using a position-sensitive silicon Oak Ridge Rutgers University Barrel Array (ORRUBA) detector that had been designed and built by the SSAA Center. The experiment was performed at the Oak Ridge National Laboratory Holifield Radioactive Ion Beam Facility and used a technique known as inverse kinematics.

First-Ever White Dwarf Star Experiment at Z

On April 14, spectra were measured from a gas cell that was the first macroscopic white dwarf star experiment ever attempted. It was a huge success on the first try. The cell was filled with 19mL of hydrogen-like gas to simulate plasma conditions in a white dwarf star.

Accurate First-Principles Prediction of Unreacted Shock Hugoniot for a High Explosive

A multi-disciplinary research team at Sandia National Laboratories (SNL) successfully used density functional theory (DFT)-based molecular dynamics (MD) calculations to determine points on the unreacted shock Hugoniot for high explosives in regimes that are difficult to probe by experiment. This effort was driven by the need to model chip-slapper neutron-generator detonator performance in weapons systems. Initial results were presented at the 14th International Detonation Symposium (IDS) the week of April 12, 2010 at Coeur d'Alene Resort in Idaho. Also presented at the IDS were new independent experimental results from Lawrence Livermore National Laboratory that confirm the DFT-MD predictions. The SNL team consisted of R.R. Wixom, A.E. Mattsson, and T.R. Mattsson.

George T. "Rusty" Gray III became the 54th president of The Minerals, Metals & Materials Society (TMS) during the 139th TMS Annual Meeting and Exhibition held in March. Rusty, as Los Alamos National Laboratory fellow is a major contributor to the Science Campaign and the DOE/DoD Joint Munitions Programs.

Evgeny Stambulchik received the 2010 IEEE Nuclear and Plasma Sciences Society Early Achievement Award. He received the award "for outstanding contributions to spectral line broadening theory and modeling, including development of numerical methods, and their applications to novel approaches in plasma diagnostics."

Physicist Omar Hurricane was named a winner of DOE's prestigious Ernest Orlando Lawrence Award. This award honors mid career scientists and engineers for exceptional contributions in research and development supporting DOE/NNSA and its missions. Hurricane was honored for his work in national security and nonproliferation.

The Naval Research Laboratory's Jack Davis joined an elite group of career senior executives when he was awarded a 2009 Presidential Rank Award, Meritorious Executive. He received the award for his leadership and exceptional and sustained accomplishments. Davis' long-term contributions to NNSA in radiation hydrodynamics and the Nuclear Weapons Enterprise are considerable.